Composite Structures 96 (2013) 243–255

Contents lists available at SciVerse ScienceDirect

Composite Structures

journal homepage: www.elsevier.com/locate/compstruct

Non-linear dynamic analysis of a sandwich beam with pseudoelastic SMA hybrid composite faces based on higher order finite element theory

S.M.R. Khalili [a,*], M. Botshekanan Dehkordi [a], E. Carrera [b], M. Shariyat [a]

[a] Center of Excellence for Research in Advanced Materials and Structures, Faculty of Mechanical Engineering, K.N. Toosi University of Technology, Tehran, Iran
[b] Department of Mechanical and Aerospace Engineering, Politecnico di Torino, Corso Duca degli Abruzzi 24, 10129 Torino, Italy

ARTICLE INFO

Article history:
Available online 18 August 2012

Keywords:
Suppression of vibration
Shape memory alloys
Material non-linearity
High order finite element
Non-linear dynamic analysis
Composite sandwich beam

ABSTRACT

In the present work a non-linear dynamic response of a continuous sandwich beam with SMA hybrid composite face sheets and flexible core is analyzed taking into account the phase transformation and also the material non-linearity effects, for every point along the face sheets. The one-dimensional constitutive equation of SMA proposed by Brinson is employed. Equations of motion are derived using Hamilton's principle and a new finite element is proposed based on a higher order sandwich panel theory. Due to the phase transformation, the equations of motion are coupled with the phase transformation's kinetic equations of SMA wires. A new finite-element-based approach along with an iterative incremental method is developed to study the dynamic response of sandwich beam with SMA hybrid composite face sheets and flexible core. A damped response of the sandwich beam is observed, which is due to the hysteresis behavior of SMA wires. The influence of the SMA wires on the vibration suppression related to the resonance phenomena of a sandwich beam as well as the effect of the through thickness location of the SMA wires inside the composite face sheets and also the effect of different boundary conditions on the dynamic response are analyzed.

© 2012 Elsevier Ltd. All rights reserved.

1. Introduction

The use of shape memory alloys (SMAs) as smart materials has been investigated extensively over the past two decades. Unlike the traditional materials or even most of the engineering material systems, SMAs can undergo a reversible phase transformation between a martensite and an austenite phases under thermo-mechanical loading. Due to this transformation, SMAs have some unique properties, such as superelasticity, high damping capability and recovery effects which lead to their wide use in the mechanical and aerospace engineering components.

However, it is important to study the behavior of shape memory alloy structures under dynamic loading. Due to having non-linear hysteresis behavior which is a result of the phase transformation, it is difficult to present a comprehensive and effective mathematical model for these structures. Hence, in the most cases the suggested models are limited to application of numerous simplifications. Hashemi and Khadem [1] studied the vibration behavior of shape memory alloy beam. They modeled the whole beam as a one-degree-of freedom system, taking into account the phase transformation effects. In a research conducted by Jafari and Ghiasvand [2], dynamic response of pseudoelastic SMA beam to a moving load was analyzed. In their study, the effect of dissipation energy was considered in terms of an equivalent damping ratio. Zbiciak [3] studied the response of SMA beam subjected to impulse loading, based on the rheological model of SMA material. In his research, the material properties were assumed to be constant and also the phase transformation was not considered.

In recent years, considerable attention has been devoted to the use of SMA wires in the fiber reinforced plastic materials to form adaptive composite structures. Rogers and Barker [4] embedded SMA wires in a graphite–epoxy composite beam to control its frequency. When the SMA wires were heated, the beam was subjected to an axial stress due to the shape memory effect (SME). They found a significant increase in the natural frequency of a graphite–epoxy beam by using 15% volume fraction of SMA wires. Baz et al. [5] mechanically connected SMA wires to the external surface of flexible beams for their active vibration control. They demonstrated the feasibility of utilizing shape memory actuators in controlling the flexural vibrations of a flexible cantilevered beam. Baz et al. [6] investigated the effects of SMA embedded in a composite beam to control its buckling and vibration behavior. They showed that the buckling load of a flexible glass fiber composite beam can be increased up to 300% over that of an uncontrolled beam. A closed-form solution for active vibration control

* Corresponding author. Address: Faculty of Mechanical Engineering, K.N. Toosi University of Technology, Pardis St., Molasadra Ave., Vanak Sq., Tehran, Iran. Tel./fax: +98 2188674747.

E-mail addresses: smrkhalili2005@gmail.com (S.M.R. Khalili), mbd_dehkordi@yahoo.com (M. Botshekanan Dehkordi), erasmo.carrera@polito.it (E. Carrera), m_shariyat@yahoo.com (M. Shariyat).

0263-8223/$ - see front matter © 2012 Elsevier Ltd. All rights reserved.
http://dx.doi.org/10.1016/j.compstruct.2012.08.020

of a flexible beam with SMA layers was proposed by Chen and Levy [7]. They used the Euler–Bernoulli beam theory to model the SMA composite beam. However, they did not consider SMA hysteresis. Epps and Chandra [8] conducted an experimental–analytical study on the active tuning of composite beams using shape memory alloy wires. They showed that the natural frequency of SMA graphite epoxy composite beams increased by increasing the number of wires. However, the details on damping properties of composite beam were not addressed. Ghomshei et al. [9] analyzed the passive as well as active vibration control of thick beam embedded with SMA ribbon. They used the shape memory effect of SMA ribbon to improve the beam's performance. Khalili et al. [10,11] investigated the effect of some important parameters on low-velocity impact response of the active thin-walled hybrid composite plates embedded with the shape memory alloy wires, employing the first order shear deformation theory as well as the Fourier series method. Lu et al. [12] proposed a theoretical model for the bending of a laminated beam with SMA fiber embedded layer. They obtained the constitutive relations of the SMA layer using the method of micromechanics.

Recently, the application of sandwich beams as primary members or structures with low weight and high strength and stiffness has widespread in various industries. The cores of the mentioned structures that are usually fabricated from light and soft materials, beside their functional characteristics, serve as spacers. Therefore, they may enhance the overall performance of the structure without increasing the total weight of the structure or complicating the manufacturing process considerably. Sandwich beams with stiff sheets and soft low strength cores have been widely used in construction of many components in automotive, aerospace, aeronautic, ship, under water and building structures. In this regard, many works have done by researchers to model the sandwich structures. Carrera and Brischetto [13] have assessed the accuracy of theories proposed for the sandwich and multilayered structures. Noor et al. [14] reviewed more than 800 papers on sandwich and multilayered structure modelings.

Widespread use of polymer foam materials as cores in sandwich structures requires application of an enhanced theory that accounts for the vertical flexibility of soft foam cores. In the most cases, the dynamic analysis of sandwich beams with soft cores has been studied using the incompressible core hypothesis [15–20]. Ditaranto [15] and Mead and Markus [16] are the earliest investigators who studied the free vibration of sandwich beams using the classical theory. A simple model assumes that the top and the bottom face sheets of a sandwich beam deform according to the Bernoulli–Euler beam theory, whereas the core deforms only in shear. This model was used by many researchers. Frostig and Baruch [21] presented different model for sandwich beams analysis. They were analyzed the free vibrations of sandwich beams with flexible core based on the high-order theory. In this model, the axial and the transverse displacements of the core were obtained by two and three order polynomials, respectively [21,22]. Many authors have investigated the high-order free vibration of sandwich beams [21–27]. Sokolinsky et al. [24] predicated the natural frequencies and corresponding vibration modes of a cantilever sandwich beam with a soft polymer core using the higher-order theory, two-dimensional finite element analysis and the experimental measurements. The comparison of their results with experimental results and those obtained using the classical formulation of Mead and Markus [16] showed the superiority of the high-order formulation. Khalili et al. [25] and Malekzadeh et al. [26] used the higher-order theory to study the low-velocity response and the local and global damped vibrations of sandwich panels. Yang and Qiao [27] presented a higher-order impact model to simulate the response of a soft-core sandwich beam subjected to a foreign object impact. Before the impact analysis, they presented the three higher-order models of sandwich beam that the dynamic effect of the core was different in them.

Very limited studies devoted on the sandwich structures embedded with SMA wires. For example, Birman [28] showed that the buckling load of the sandwich panel increased by using the shape memory effect of the SMA wires. SMA wires were embedded at the mid-plane of the core. In his research, the first shear deformation theory is used to model the panel. The phase transformation of the SMA wires were not considered and the material properties of the SMA wires were assumed to be constant.

Vibration control in the sandwich panels is an important issue. Sometimes, this task may be accomplished by addition of viscoelastic constrained layer for damping treatments. However, in some applications there are some limitations in using these layers. Shape memory alloy materials are good candidates for damping vibration systems. Presence of hysteresis during austenite and martensite phase transformations yields an acceptable energy loss capacity. Furthermore, shape memory alloys materials have the unusual (pseudoelastic) material property able to sustain and recover large strains (of the order of 10%) without inducing irreversible plastic deformation [29].

As mentioned before, many researches have been devoted to the composite beams embedded with SMA wires (that are limited to application of numerous simplifications). But, to best knowledge of the authors, there is no study of the sandwich beam with SMA composite hybrid face sheets.

In this paper, the non-linear dynamic response of continuous sandwich beam with pseudoelastic SMA hybrid composite face sheets is investigated for the first time. SMA wires are assumed to be embedded in the composite layers of the face sheets to improve the damping performance of composite beam. What makes the present study different from the previous works is that, the non-linear dynamic response of the sandwich beam embedded with SMA wires is investigated for the first time and also the instantaneous phase transformation effects are taken into account at all the points along the face sheets. Equations of motion are derived using Hamilton's principle based on the high order sandwich panel theory. The one-dimensional constitutive equation of SMA proposed by Brinson is employed to model the pseudoelastic behavior of SMA wires. A new element is proposed based on the high order sandwich panel theory and therefore a new finite-element–based solution procedure is developed to solve the highly non-linear equations. Finally, the problem is coded in MATLAB system for studying the dynamical response of the sandwich beam with pseudoelastic SMA hybrid composite face sheets.

2. Constitutive equation of the SMA wires

In the present study, the one-dimensional constitutive equation of SMA has been derived by Brinson is employed. The constitutive equation by Brinson [30] relates the stress (σ) to the strain (ε), temperature (T) and martensite fraction (ξ) in the following form:

$$\sigma - \sigma_0 = E(\xi)(\varepsilon) - E(\xi_0)(\varepsilon_0) + \Omega(\xi)(\xi_s) - \Omega(\xi_0)(\xi_{s0}) + \theta(T - T_0) \tag{1}$$

where $E(\xi)$, θ and $\Omega(\xi)$ are the Young's modulus, the thermoelastic tensor, and the transformation tensor, respectively. The terms associated with subscript "o" refer to the initial conditions. In addition, $E(\xi)$ and $\Omega(\xi)$ can be expressed as:

$$E(\xi) = E_A + \xi(E_M - E_A) \tag{2a}$$

$$\Omega(\xi) = -\varepsilon_L E(\xi) \tag{2b}$$

where E_A and E_M are the Young's modulus of SMA in austenite and martensite phases, respectively and ε_L is the maximum recoverable

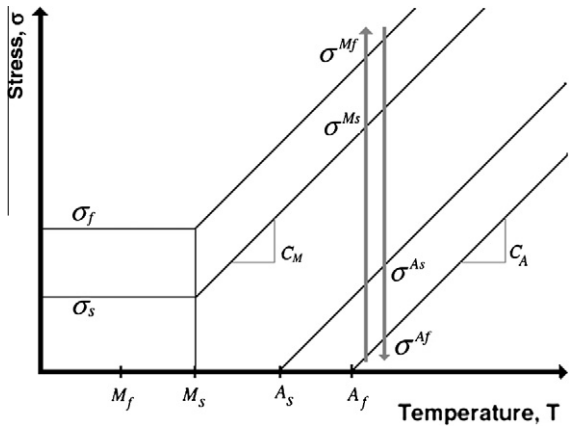

Fig. 1. Pseudoelastic loading–unloading path [31].

strain. In this model, a modified cosine model for the martensite volume fraction is divided into two parts.

$$\xi = \xi_s + \xi_T \tag{3}$$

where ξ_s represents the fraction of the material that is stress-induced martensite with single variants, and ξ_T denotes the fraction of the material that is temperature-induced martensite with multiple variant.

Phase transformation's kinetic equations in conjunction with Fig. 1 is presented as:

2.1. Conversion to detwinned martensite

For $T > M_s$ and $\sigma_s^{cr} + C_M(T - M_s) < \sigma < \sigma_f^{cr} + C_M(T - M_s)$

$$\xi_s = \frac{1-\xi_{s0}}{2}\cos\left(\frac{\pi}{\sigma_s^{cr}-\sigma_f^{cr}}\left(\sigma-\sigma_f^{cr}-C_M(T-M_s)\right)\right)+\frac{1+\xi_{s0}}{2}$$

$$\xi_T = \xi_{T0} - \frac{\xi_{T0}}{1-\xi_{s0}}(\xi_s - \xi_{s0}) \tag{4a}$$

For $T < M_s$ and $\sigma_s^{cr} < \sigma < \sigma_f^{cr}$

$$\xi_s = \frac{1-\xi_{s0}}{2}\cos\left(\frac{\pi}{\sigma_s^{cr}-\sigma_f^{cr}}\left(\sigma-\sigma_f^{cr}\right)\right)+\frac{1+\xi_{s0}}{2} \tag{4b}$$

$$\xi_T = \xi_{T0} - \frac{\xi_{T0}}{1-\xi_{s0}}(\xi_s - \xi_{s0}) + \Delta_{T\xi}$$

For $M_f < T < M_s$ and $T < T_0$

$$\Delta_{T\xi} = \frac{1-\xi_{T0}}{2}(\cos(a_M(T-M_f))+1)$$

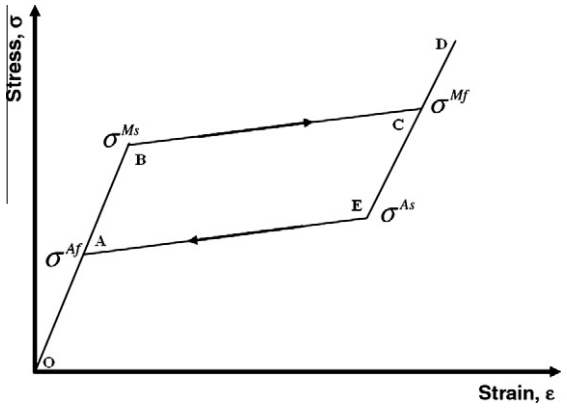

Fig. 2. Schematic of a pseudoelastic stress–strain diagram [31].

Else $\Delta_{T\xi} = 0$

2.2. Conversion to austenite

For $T > A_s$ and $C_A(T - A_f) < \sigma < C_A(T - A_s)$

$$\xi = \frac{\xi_{s0}}{2}\cos\left(a_A\left(T - A_s - \frac{\sigma}{C_A}\right)+1\right) \tag{4c}$$

$$\xi_s = \xi_{s0} - \frac{\xi_{s0}}{\xi_0}(\xi_0 - \xi)$$

$$\xi_T = \xi_{T0} - \frac{\xi_{T0}}{\xi_0}(\xi_0 - \xi)$$

In the above equations, σ_s^{cr} is the critical stress for the start of transformation and σ_f^{cr} is the critical stress at the end of transformation. All shape memory alloys have characteristic stress–strain curves. For example, a typical stress–strain curve of SMA in tension with pseudoelastic effect is shown in Fig. 2. Three distinct stages are observed: for stresses below σ^{Ms} (line OB in Fig. 2), the material behaves in a purely elastic way in the austenite phase. When the critical stress is reached (e.g., point B in Fig. 2), forward transformation (austenite-to-martensite) initiates and the stress-induced martensite starts forming (line BC in Fig. 2). During the formation of martensite, large transformation strains are generated (upper plateau of stress–strain curve). When the applied stress reaches the value of σ^{Mf}, the forward transformation is completed and the SMA is in the martensitic phase. For further loading above σ^{Mf} (e.g., line CD in Fig. 2) the elastic behavior of martensite is observed. During unloading from point D up to point E, the elastic behavior is observed. Upon further unloading, the reverse transformation of martensite into austenite initiates at a stress σ^{As} and completes at a stress σ^{Af} (line EA in Fig. 2). As can be seen, a hysteresis loop is obtained in the loading/unloading stress–strain diagram due to the difference between σ^{Mf} and σ^{As} and between σ^{Ms} and σ^{Af}. This hysteresis loop is causing a damping phenomenon to the structures especially in the dynamic problems.

3. Theoretical formulation and methods

The equations of motions of the SMA-sandwich beam are derived through the Hamilton's principle based on the high order sandwich panel theory [21], which extremizes the Lagragian as follows [32]:

$$\int_{t_1}^{t_2}(-\delta T + \delta V + \delta U)dt = 0 \tag{5}$$

where T, U and V are kinetic energy, internal potential energy and external potential energy respectively; t is the time coordinate that varies between the times t_1 and t_2, that is, the initial and the final time, respectively; and δ denotes the variational operator. Consider a sandwich beam of length L and width b, consisting of a core with thickness h_c, Young's and shear modulus E_c and G_c, respectively, and two SMA-embedded composite face sheets with the thicknesses of h_t and h_b, as shown in Fig. 3. Subscripts and denote the top and the bottom face sheets, respectively.

The first variation of the kinetic energy for the sandwich beam reads:

$$\delta T = \int_0^L \int_{-\frac{h_t}{2}}^{\frac{h_t}{2}}(\rho_t \dot{u}_t \delta u_t + \rho_t \dot{w}_t \delta w_t)dz_t\,dx + \int_0^L \int_{-\frac{h_b}{2}}^{\frac{h_b}{2}}(\rho_b \dot{u}_b \delta u_b + \rho_b \dot{w}_b \delta w_b)dz_b\,dx + \int_0^L \int_0^{h_c}(\rho_c \dot{u}_c \delta u_c + \rho_c \dot{w}_c \delta w_c)dz_c\,dx \tag{6}$$

where ρ_j ($j = t, b, c$) are the mass per area of the top and the bottom face sheets and the core respectively; z_t, z_b and z_c are the vertical coordinate of the top and the bottom face sheets and the core,

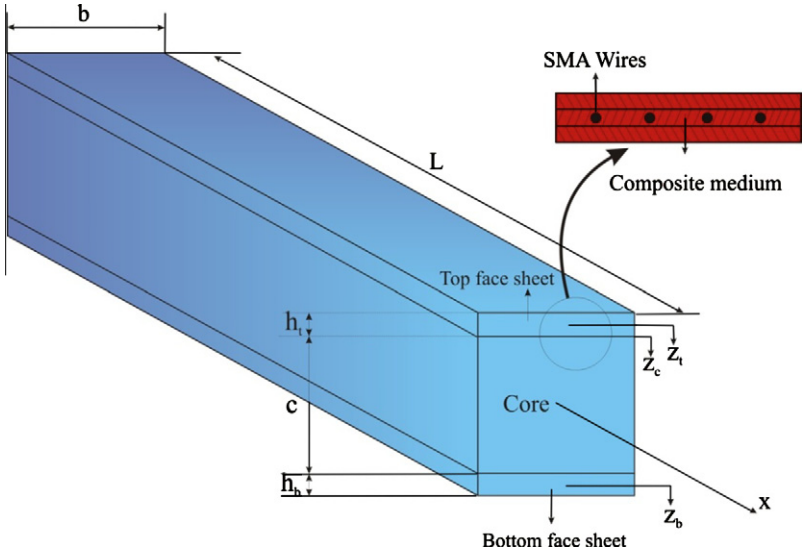

Fig. 3. Geometry and coordinate systems of the sandwich beam with SMA hybrid composite face sheets.

respectively; u_j and w_j ($j = t, b, c$) are the displacements in longitudinal and vertical directions, respectively; $\dot{u}_j$ and $\dot{w}$ ($j = t, b, c$) are the velocities in longitudinal and vertical directions, respectively, for the sandwich beam constituents.

The first variation of the external potential energy for the sandwich beam reads:

$$\delta V = \int_0^L (q_t \delta w_t + q_b \delta w_b) dx \tag{7}$$

where q_j ($j = t, b$) are the vertical distributed loads over the top and the bottom face sheets, respectively. The total internal potential energy is given by the mechanical potential energy and the potential energy due to the phase transformation:

$$\delta U = \delta U_M + \delta U_s \tag{8}$$

where, U_M is the strain energy due to the mechanical stresses and U_s is the potential energy due to the phase transformation of SMA wires. The δU_M is given by:

$$\delta U_M = \int_{V_t} \sigma^t_{xxM} \delta \varepsilon^t_{xx} dV + \int_{V_b} \sigma^b_{xxM} \delta \varepsilon^b_{xx} dV + \int_{V_c} (\tau^c_{xz} \delta \gamma^c_{xz} + \sigma^c_{zz} \delta \varepsilon^c_{zz}) dV \tag{9}$$

where σ^j_{xxM} and $\varepsilon^j_{xx} (j = t, b)$ are the in-plane normal stresses and strains in the top and the bottom face sheets; τ^c_{xz} and γ^c_{xz} are the vertical shear stress and strain in the flexible core; and σ^c_{zz}, ε^c_{zz} are the normal stresses and strains in the vertical direction of the core. Due to the low strength of the core in the axial direction, the axial normal stress of the core is negligible. τ^c_{xz} and V_j ($j = t, b, c$) are the volume of the top and the bottom sheets and the core, respectively. The displacements pattern of the face sheets ($j = t, b$) following the classical Bernoulli assumptions, the kinematic relations corresponding to small linear displacements of the face sheets and the core, and the compatibility conditions at the upper and the lower face–core interfaces equal:

$$u_j(\xi) = u_{0j}(\xi) - z_j \frac{\partial w_j(\xi)}{\partial x} \tag{10}$$

$$\varepsilon^j_{xx}(\xi) = \frac{\partial u_{0j}(\xi)}{\partial x} - z_j \frac{\partial^2 w_j(\xi)}{\partial x^2} \tag{11}$$

$$\varepsilon^c_{zz}(\xi) = \frac{\partial w_c(\xi)}{\partial z} \quad \gamma^c_{xz}(\xi) = \frac{\partial u_c(\xi)}{\partial z} + \frac{\partial w_c(\xi)}{\partial x} \tag{12}$$

$$u_c(x, z_c = 0) = u_{0t} - \frac{h_t}{2} \frac{\partial w_t(\xi)}{\partial x} \tag{13a}$$

$$w_c(x, z_c = 0) = w_t \tag{13b}$$

$$u_c(x, z_c = c) = u_{0b} + \frac{h_b}{2} \frac{\partial w_b(\xi)}{\partial x} \tag{14a}$$

$$w_c(x, z_c = c) = w_b \tag{14b}$$

The δU_s is given by:

$$\delta U_s = \int_{V_t} \sigma^t_{xxs} \delta \varepsilon^t_{xx} dV + \int_{V_b} \sigma^b_{xxs} \delta \varepsilon^b_{xx} dV \tag{15}$$

where $\sigma^j_{xxs} (j = t, b)$ are the stresses due to the phase transformation in the top and bottom face sheets that can be defined by:

$$\sigma^{kj}_{xxs}(\xi) = k^{kj}_s \chi^{kj}_s \tag{16}$$

where k^{kj}_s represents the volume fraction of the SMA wires in the kth layer of the SMA hybrid composite face sheets. The entry of χ^{kj}_s, which is due to the phase transformation in the SMA wires, is defined by:

$$\chi^{kj}_s(\xi) = -\varepsilon_L E^{kj}_s (\xi^{kj}) \xi^{kj} \tag{17}$$

where ξ^{kj} and E^{kj}_s are the martensite volume fraction and the Young's modulus of the SMA wires of the kth layer, respectively.

Using the Hamilton's principle, Eq. (5), the expression of the kinetic energy, the external potential energy and the internal potential energy, Eqs. (6)–(9) and Eqs. (15)–(17), along with the assumption of the linear acceleration distribution, the kinematic relations of the face sheets and the core, (10)–(12), the compatibility conditions corresponding to perfect bonding at the face sheet–core interfaces, Eqs. (13) and (14), and after some algebraic manipulation, the equations of motion are as follows:

$$\frac{\partial N^t_{xx}(\xi)}{\partial x} + \frac{\partial A^t_{xxs}(\xi)}{\partial x} + \tau_{xz} b - I_{0t} \ddot{u}_{0t} + I_{1t} \frac{\partial \ddot{w}_t}{\partial x} - \frac{m_c}{6} \ddot{u}_{0b} - \frac{m_c h_b}{12} \frac{\partial \ddot{w}_b}{\partial x} - \frac{m_c}{3} \ddot{u}_{0t} + \frac{m_c h_t}{6} \frac{\partial \ddot{w}_t}{\partial x} = 0 \tag{18}$$

$$\frac{\partial N^b_{xx}(\xi)}{\partial x} + \frac{\partial A^b_{xxs}(\xi)}{\partial x} - \tau_{xz} b - I_{0b} \ddot{u}_{0b} + I_{1b} \frac{\partial \ddot{w}_b}{\partial x} - \frac{m_c}{3} \ddot{u}_{0b} - \frac{m_c h_b}{6} \frac{\partial \ddot{w}_b}{\partial x} - \frac{m_c}{6} \ddot{u}_{0t} + \frac{m_c h_t}{12} \frac{\partial \ddot{w}_t}{\partial x} = 0 \tag{19}$$

$$\frac{\partial^2 M^t_{xx}(\xi)}{\partial x^2}+\frac{\partial^2 B^t_{xxs}(\xi)}{\partial x^2}+\frac{bh_t}{2}\frac{\partial \tau^c_{xz}}{\partial x}+b\sigma^c_{zz}(z_c=0)-I_{0t}\ddot{w}_t-I_{1t}\frac{\partial \ddot{u}_{0t}}{\partial x}+I_{2t}\frac{\partial^2 \ddot{w}_t}{\partial x^2}-\frac{m_c h_t}{12}\frac{\partial \ddot{u}_{0b}}{\partial x}-\frac{m_c h_t h_b}{24}\frac{\partial^2 \ddot{w}_b}{\partial x^2}-\frac{m_c h_t}{6}\frac{\partial \ddot{u}_{0t}}{\partial x}+\frac{m_c h_t^2}{12}\frac{\partial^2 \ddot{w}_t}{\partial x^2}-\frac{m_c}{6}\ddot{w}_b-\frac{m_c}{3}\ddot{w}_t+q_t(t)=0 \tag{20}$$

$$\frac{\partial^2 M^b_{xx}(\xi)}{\partial x^2}+\frac{\partial^2 B^b_{xxs}(\xi)}{\partial x^2}+\frac{bh_b}{2}\frac{\partial \tau^c_{xz}}{\partial x}-b\sigma^c_{zz}(z_c=c)-I_{0b}\ddot{w}_b-I_{1b}\frac{\partial \ddot{u}_{0b}}{\partial x}+I_{2b}\frac{\partial^2 \ddot{w}_b}{\partial x^2}+\frac{m_c h_b}{6}\frac{\partial \ddot{u}_{0b}}{\partial x}+\frac{m_c h_b^2}{12}\frac{\partial^2 \ddot{w}_b}{\partial x^2}+\frac{m_c h_b}{12}\frac{\partial \ddot{u}_{0t}}{\partial x}-\frac{m_c h_t h_b}{24}\frac{\partial^2 \ddot{w}_t}{\partial x^2}-\frac{m_c}{3}\ddot{w}_b-\frac{m_c}{6}\ddot{w}_t+q_b(t)=0 \tag{21}$$

$$\tau^c_{xz,z_c}=0,\quad \tau^c_{xz,x}+\sigma^c_{zz,z_c}=0 \tag{22}$$

where I_{ij} ($i=1,2,3$; $j=t$ and b) are the mass moment of inertia per unit length, of the top and the bottom face sheets; M_c is the mass per unit length of the core; $N^j_{xx}(\xi)(j=t,b)$ are the normal stress resultants in the longitudinal direction at the top and the bottom face sheets; $M^j_{xx}(\xi)(j=t,b)$ are the bending moment resultants in the longitudinal direction at various face sheets; τ^c_{xz} and τ^c_{zz} are the shear stress and the vertical normal stress at the flexible core, respectively.

Normal stress resultants and moment resultants at the face sheets can be expressed as:

$$\begin{bmatrix} N^j_{xx}(\xi) \\ M^j_{xx}(\xi) \end{bmatrix}=\sum_{kj=1}^{Nkj}\int_{z_{j,k}}^{z_{j,k+1}}\sigma^{kj}_{xx}(\xi)\begin{pmatrix}1\\ z_j\end{pmatrix}dz_j \tag{23}$$

The stresses in Eq. (23) can be related to the total strain by:

$$\sigma^{kj}_{xx}(\xi)=Q^{kj}(\xi)\left(\frac{\partial u_{0j}(\xi)}{\partial x}-z_j\frac{\partial^2 w_j(\xi)}{\partial x^2}\right) \tag{24}$$

where Q^{kj} represents the stiffness for the SMA hybrid composite of the kth ply of the face sheets. The material properties of a SMA hybrid composite ply are achieved by the following relations [33]:

$$E_l(\xi)=E^c_l k_c+E_s(\xi)k_s \tag{25a}$$

$$E_t(\xi)=E^c_t\Big/\left(1-\sqrt{k_s}(1-E^c_t/E_s(\xi))\right) \tag{25b}$$

$$G_{lt}(\xi)=G^c_{lt}G_s(\xi)/(k_cG_s(\xi)+k_sG^c_{lt}) \tag{25c}$$

$$\upsilon_{lt}=\upsilon^c_{lt}k_c+\upsilon_s k_s \tag{25d}$$

where subscript 's' and superscript 'c' identify the shape memory and the composite medium material, respectively. Based on Eqs. (10), (11) and (24), the stress resultants and the bending moment resultants can be expressed as:

$$N^j_{xx}(\xi)=A^j(\xi)\frac{\partial u_{0j}(\xi)}{\partial x}+B^j(\xi)\frac{\partial^2 w_j(\xi)}{\partial x^2} \tag{26a}$$

$$M^j_{xx}(\xi)=B^j(\xi)\frac{\partial u_{0j}(\xi)}{\partial x}+D^j(\xi)\frac{\partial^2 w_j(\xi)}{\partial x^2} \tag{26b}$$

where A^j, B^j and D^j are the extensional stiffness, the coupling stiffness and the bending stiffness of the face sheets, respectively. In addition, the entries of A^j_{xxx} and B^j_{xxx} which are due to the phase transformation in the SMA wires, can be defined as $j=t$, b:

$$A^j_{xxs}(\xi)=\sum_{k=1}^{klj}bk^{kj}_s\chi^{kj}_s(\xi)(z_{j,k+1}-z_{j,k}) \tag{27a}$$

$$B^j_{xxs}(\xi)=1/2\sum_{k=1}^{klj}bk^{kj}_s\chi^{kj}_s(\xi)(z^2_{j,k+1}-z^2_{j,k}) \tag{27b}$$

The derivation of the non-linear displacements and the stress fields in the flexible core has been described in detail in Ref. [34]. For the sake of brevity, only the final results are presented here:

$$u_c(x,z_c)=\frac{1}{2E_c}\frac{\partial^2 \tau^c_{xz}}{\partial x^2}\left(\frac{z_c^3}{3}-\frac{z_c^2 c}{2}\right)+\frac{\tau^c_{xz}z_c}{G_c}-\frac{z_c^2}{2c}\frac{\partial w_b}{\partial x}+\frac{\partial w_t}{\partial x}\left(\frac{z_c^2}{2c}-z_c-\frac{h_t}{2}\right)+u_{ot} \tag{28a}$$

$$w_c(x,z_c)=-\frac{1}{2E_c}\frac{\partial \tau^c_{xz}}{\partial x}z_c^2+\frac{1}{2E_c}\frac{\partial \tau^c_{xz}}{\partial x}z_c c+\frac{z_c}{c}(w_b-w_t)+w_t \tag{28b}$$

$$\sigma^c_{zz}(x,z_c)=-\frac{1}{2}\frac{\partial \tau^c_{xz}}{\partial x}(2z_c-c)+\frac{E_c}{c}(w_b-w_t) \tag{28c}$$

The governing equations of motion are obtained using Eqs. (18)–(21) and Eq. (26). The last equation is derived using the compatibility requirements at the lower face–core interface in the x direction, Eq. (14a). Hence, the governing equations of motion can be expressed as:

$$\frac{\partial}{\partial x}\left(A^t(\xi)\frac{\partial u_{0t}(\xi)}{\partial x}+B^t(\xi)\frac{\partial^2 w_t(\xi)}{\partial x^2}\right)+\frac{\partial A^t_{xxs}(\xi)}{\partial x}+\tau_{xz}b-I_{0t}\ddot{u}_{0t}+I_{1t}\frac{\partial \ddot{w}_t}{\partial x}-\frac{m_c}{6}\ddot{u}_{0b}-\frac{m_c h_b}{12}\frac{\partial \ddot{w}_b}{\partial x}-\frac{m_c}{3}\ddot{u}_{0t}+\frac{m_c h_t}{6}\frac{\partial \ddot{w}_t}{\partial x}=0 \tag{29}$$

$$\frac{\partial}{\partial x}\left(A^b(\xi)\frac{\partial u_{0b}(\xi)}{\partial x}+B^b(\xi)\frac{\partial^2 w_b(\xi)}{\partial x^2}\right)+\frac{\partial A^b_{xxs}(\xi)}{\partial x}-\tau_{xz}b-I_{0b}\ddot{u}_{0b}+I_{1b}\frac{\partial \ddot{w}_b}{\partial x}-\frac{m_c}{3}\ddot{u}_{0b}-\frac{m_c h_b}{6}\frac{\partial \ddot{w}_b}{\partial x}-\frac{m_c}{6}\ddot{u}_{0t}+\frac{m_c h_t}{12}\frac{\partial \ddot{w}_t}{\partial x}=0 \tag{30}$$

$$\frac{\partial^2}{\partial x^2}\left(B^t(\xi)\frac{\partial u_{0t}(\xi)}{\partial x}+D^t(\xi)\frac{\partial^2 w_t(\xi)}{\partial x^2}\right)+\frac{\partial^2 B^t_{xxs}(\xi)}{\partial x^2}+\frac{bh_t}{2}\frac{\partial \tau^c_{xz}}{\partial x}+\frac{bE_c}{c}(w_b-w_t)+\frac{cb}{2}\frac{\partial \tau^c_{xz}}{\partial x}-I_{0t}\ddot{w}_t-I_{1t}\frac{\partial \ddot{u}_{0t}}{\partial x}+I_{2t}\frac{\partial^2 \ddot{w}_t}{\partial x^2}-\frac{m_c h_t}{12}\frac{\partial \ddot{u}_{0b}}{\partial x}-\frac{m_c h_t h_b}{24}\frac{\partial^2 \ddot{w}_b}{\partial x^2}-\frac{m_c h_t}{6}\frac{\partial \ddot{u}_{0t}}{\partial x}+\frac{m_c h_t^2}{12}\frac{\partial^2 \ddot{w}_t}{\partial x^2}-\frac{m_c}{6}\ddot{w}_b-\frac{m_c}{3}\ddot{w}_t+q_t(t)=0 \tag{31}$$

$$\frac{\partial^2}{\partial x^2}\left(B^b(\xi)\frac{\partial u_{0b}(\xi)}{\partial x}+D^b(\xi)\frac{\partial^2 w_b(\xi)}{\partial x^2}\right)+\frac{\partial^2 B^b_{xxs}(\xi)}{\partial x^2}+\frac{bh_b}{2}\frac{\partial \tau^c_{xz}}{\partial x}-\frac{bE_c}{c}(w_b-w_t)+\frac{cb}{2}\frac{\partial \tau^c_{xz}}{\partial x}-I_{0b}\ddot{w}_b-I_{1b}\frac{\partial \ddot{u}_{0b}}{\partial x}+I_{2b}\frac{\partial^2 \ddot{w}_b}{\partial x^2}+\frac{m_c h_b}{6}\frac{\partial \ddot{u}_{0b}}{\partial x}+\frac{m_c h_b^2}{12}\frac{\partial^2 \ddot{w}_b}{\partial x^2}+\frac{m_c h_b}{12}\frac{\partial \ddot{u}_{0t}}{\partial x}-\frac{m_c h_t h_b}{24}\frac{\partial^2 \ddot{w}_t}{\partial x^2}-\frac{m_c}{3}\ddot{w}_b-\frac{m_c}{6}\ddot{w}_t+q_b(t)=0 \tag{32}$$

$$u_{0t}-u_{0b}-\frac{c^3}{12E_c}\frac{\partial^2 \tau^c_{xz}}{\partial x^2}+\frac{\tau^c_{xz}c}{G_c}-\frac{(c+h_t)}{2}\frac{\partial w_t}{\partial x}-\frac{(c+h_b)}{2}\frac{\partial w_b}{\partial x}=0 \tag{33}$$

According to the governing equations of motion, it can be seen that its coefficients and also some parameters are dependent on the martensite volume fraction and therefore, these coefficients and parameters are dependent on the time and the location of any point along the face sheets. Meanwhile, with respect to the martensite volume fraction dependency on the stress and subsequently the displacement values, these coefficients are unknown. Therefore, in this study not only are the material properties variable with respect to the time and the location; they are also unknown. Therefore, the equations of motion and the phase transformation's kinetic equations are coupled together, which makes the problem more complicated.

3.1. Finite element modeling

To investigate the dynamic response of the SMA hybrid composite sandwich beam, a new transient finite element model is developed. The Galerkin weighted-residual method (in the finite element context) is used to obtain the finite element characteristics for the high-order beam element. The finite element governing equations of the beam can be derived from Eqs. (29)–(33) using the proposed high-order sandwich beam element. It is known that the order of the differentiating operator of the transverse displacement component is higher in comparison with the in-plane displacement component. Moreover, for more accurate results, the continuity of the slope in the beam must be guaranteed. For these reasons, the transverse displacement components must be C^1-continuous. Therefore, compatible Hermite cubic shape functions are employed to interpolate the transverse displacement components. Moreover, the in-plane displacement at the face sheets and also the shear stress in the flexible core may be interpolated using Lagrange quadratic shape functions. The generalized variables are approximated by using the following interpolations:

$$u_{0j}^e = \sum_{i=1}^{3} \psi_i(s) u_{ij} \quad w_j^e = \sum_{i=1}^{4} \phi_i(s) w_{ij} \ (j = t, b) \quad \tau^e = \sum_{i=1}^{3} \psi_i(s) \tau_i \tag{34}$$

where ψ_i are the Lagrange quadratic interpolation functions and ϕ_i are the Hermite cubic interpolation functions.

Substituting Eq. (34) into equations of motion, Eqs. (29)–(33), and then using the Galerkin weighted-residual method, the semi-discretized element equation is obtained, which is in the form of a set of hyperbolic differential equations in time as follows:

$$[M^e]\{\ddot{\Delta}^e(t)\} + [K^e(\xi)]\{\Delta^e(t)\} = \{F^e(t,\xi)\} \tag{35}$$

where $[M^e]$ is the element mass matrix, $[K^e]$ is the element stiffness matrix, $\{F^e\}$ is the total force vector, and Δ^e is the vector of the nodal values. Stiffness matrix $[K]$ is composed of 5×5 sub-matrices and the mass matrix $[M]$ is composed of 4×4 sub-matrices and the elements of these sub-matrices are given in the appendix. The corresponding dimension of the element stiffness matrix is 17, and that of the mass matrix is only 14. This happens, since the last equation of motion (see Eq. (33)), that describes the compatibility conditions in the longitudinal direction at the lower face–core interface, does not contain any inertia terms. Hence, the stiffness matrix can be condensed into a dimension of the mass matrix, that is, 14. Therefore, by using the standard condensation techniques [35], the compact form of the matrix-type of the governing equations of the entire sandwich beam may be derived by eliminating the nodal degree of shear stress in Eq. (35). The element stiffness matrix and the total force vector in Eq. (35) are non-linear and asymmetric, and therefore, an incremental solution method along with an iterative scheme is employed to solve the highly non-linear dynamic equations.

The Newmark method is implemented for the integration of Eq. (35) with respect to time as follows [36]:

$$\{\Delta^e\}_{m+1} = \{\Delta^e\}_m + \Delta t\{\dot{\Delta}^e\}_m + 1/2\Delta t^2\{\ddot{\Delta}^e\}_{m+\gamma} \tag{36a}$$

$$\{\dot{\Delta}^e\}_{m+1} = \{\dot{\Delta}^e\}_m + \Delta t\{\ddot{\Delta}^e\}_{m+\alpha} \tag{36b}$$

where $\{\Delta^e\}$ and $\{\dot{\Delta}^e\}$ are respectively the element displacement vector and its first derivative with respect to time. Also,

$$\{\ddot{\Delta}^e\}_{m+\alpha} = (1-\alpha)\{\ddot{\Delta}^e\}_m + \alpha\{\ddot{\Delta}^e\}_{m+1} \tag{36c}$$

Here $\alpha = 1/2$, $\gamma = 8/5$ [36]. The set of expressions in Eq. (35) can be reduced, with the help of Eqs. (36a)–(36b), to the discretized form of the element equation, as follows:

$$[\widehat{K}^e]_{m+1}\{\Delta^e\}_{m+1} = \{\widehat{F}^e\}_{m,m+1} \tag{37}$$

where

$$[\widehat{K}^e]_{m+1} = [K^e]_{m+1} + a3[M^e]_{m+1} \tag{38a}$$

$$\{\widehat{F}^e\}_{m,m+1} = \{F^e\}_{m,m+1} + [M^e]_{m+1}(a3\{\Delta^e\}_m + a4\{\dot{\Delta}^e\}_m + a5\{\ddot{\Delta}^e\}_m) \tag{38b}$$

and a_3, a_4 and a_5 are defined as [36]:

$$a_3 = 2/(\gamma(\Delta t)^2), \quad a_4 = 2/(\gamma(\Delta t)), \quad a_5 = 1/\gamma - 1 \tag{39}$$

The initial value of acceleration is usually not known. As an approximation, it can be calculated from Eq. (35) using initial conditions on $\{\Delta^e\}_0$ and $\{F^e\}_0$ (often $\{F^e\}$ is assumed to be zero at $t = 0$):

$$\{\ddot{\Delta}^e\}_0 = [M^e]^{-1}(\{F^e\}_0 - [K^e]\{\Delta^e\}_0) \tag{40}$$

At the end of each time step, the new velocity and acceleration vectors are computed using the following equations:

$$\{\ddot{\Delta}^e\}_{m+1} = a_3(\{\Delta^e\}_{m+1} - \{\Delta^e\}_m) - a_4\{\dot{\Delta}^e\}_m - a_5\{\ddot{\Delta}^e\}_m \tag{41a}$$

$$\{\dot{\Delta}^e\}_{m+1} = \{\dot{\Delta}^e\}_m + a_2\{\ddot{\Delta}^e\}_m + a_1\{\ddot{\Delta}^e\}_{m+1} \tag{41b}$$

where $a_1 = \alpha\Delta t$ and $a_2 = (1-\alpha)\Delta t$.

3.2. The proposed numerical solution procedure

The step-by-step procedure for solving the highly non-linear system of equations is accomplished as follows:

1. Adopting initial values for $\{\Delta^e\}_0, \{\dot{\Delta}^e\}_0$ and $\{\xi\}_0^k$, (usually, zero values). Solving Eq. (40) for initial acceleration $\{\ddot{\Delta}^e\}_0$.
2. Determining the new time $t_{m+1} = t_m + \Delta t_{m+1}$ and setting $\{\xi^p\}_{m+1}^k = \{\xi\}_{m+1}^k$.
3. Computing the material properties and $\chi_s^{kj}(\xi)$ based on the $\{\xi^p\}_{m+1}^k$. Solving Eq. (37) for $\{\Delta\}_{m+1}$ using $\{\xi^p\}_{m+1}^k$.
4. Determining $\{\sigma\}_{m+1}^k$ based on the $\{\xi^p\}_{m+1}^k$ and $\{\Delta\}_{m+1}$.
5. Computing $\{\xi\}_{m+1}^k$ by the phase transformation kinetic equations using $\{\sigma\}_{m+1}^k$. (In this regard, see Fig. 4).
6. The iterative solution is continued till convergence is achieved. The following criterion may be chosen in this regard:

$$\max\left(\frac{\left|\xi_{i,m+1}^k - \xi_{i,m+1}^{kp}\right|}{\left|\xi_{i,m+1}^k\right|}\right) < \delta \tag{42}$$

   where the superscript p denote the predictor, k denote kth layer of the face sheets and represent the value of martensite volume fraction at the ith gauss quadrature point for each element. In addition, δ is a sufficiently small number. If the convergence criterion is satisfied, $\{\dot{\Delta}^e\}_{m+1}$ and $\{\ddot{\Delta}^e\}_{m+1}$ are computed using Eq. (41) and then, increment the time and repeating the steps (2)–(6). If the convergence criterion is not satisfied, determining the new estimates $\{\xi^p\}_{m+1}^k$ by using the relaxation method, as follows:
7. $\{\xi^p\}_{m+1}^k = \{\xi\}_{m+1}^k + \varsigma(\{\xi\}_{m+1}^k - \{\xi^p\}_{m+1}^k)$ and repeating the steps (3)–(6) until the convergence criterion is satisfied.

In step (5), to recognize the state of the phase transformation on each gauss quadrature point along the face sheets, the algorithm presented in Fig. 4 is used at every time increment.

4. Numerical results and discussion

A program in MATLAB is developed to derive the results based on the procedure outlined above. In order to validate the present model, some particular examples are investigated and compared with the results reported in the literature. Some examples regarding the dynamic response of SMA hybrid composite sandwich

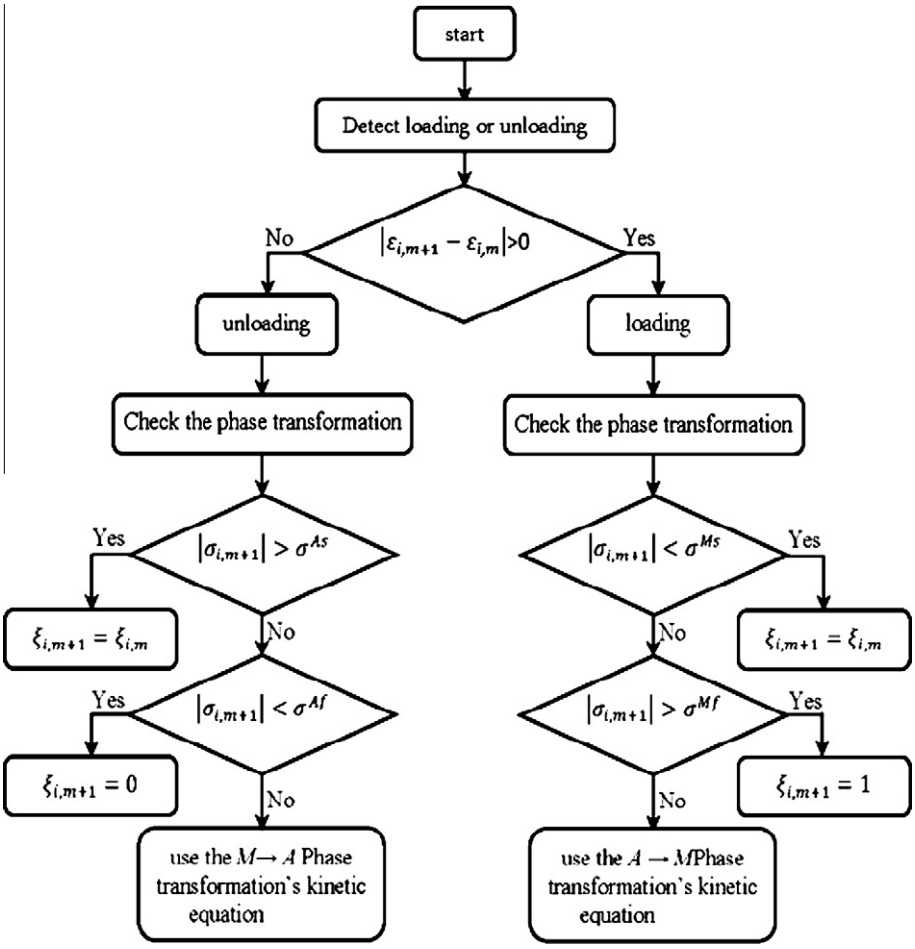

Fig. 4. Solution algorithm for the dynamic phase transformation.

beam subjected to impulse load as well as the suppression of vibrations related to resonance phenomena are also included as new results not hitherto reported in the literature.

Example 1. The high order finite element model is verified here through comparison of the simulation of the free vibration of sandwich beam with published experimental results. These experimental measurements are reported by Jensen and Irgen [37]. They examined the simply supported sandwich beam using the TV-holography technique with the following parameters:

$L = 30$ cm, $c = 3$ cm, $h_t = h_b = 0.2$ cm, $b = 5$ cm

$E_c = 56$ MPa, $G_c = 22$ MPa, $\rho_c = 60$ kg/m^3

$E_t = E_b = 210$ GPa, $\upsilon_t = \upsilon_b = 0.3$, $\rho_t = \rho_b = 7900$ kg/m^3

The comparison between the prediction of the present model and the measured vibration modes is presented in Table 1. The antisymmetric modes in Table 1 involves a displacement pattern that is antisymmetric with respect to the beam mid-height, that is, the face sheets move in phase with each other. As shown in Table 1, the greatest discrepancy between the experimental results and the present model is 4.56% which occurs for the fundamental frequency. The discrepancy arises because the specimen was slightly clamped at each support to prevent it from sliding out of the supports, as reported in Ref. [37]. However, for the higher modes, the influence of this partial clamping diminishes, and the theoretical predictions and the experiments are much closer to each other. For the reason discussed in Ref. [37], the detection of symmetric modes has presented significant difficulties. Therefore, it is not possible to compare the symmetric modes.

Table 1
Comparison of the natural frequencies of a sandwich beam with flexible core for the first five antisymmetric modes.

Mode	Experiment [37]	Present model	% Discrepancy
Frequencies (Hz)			
1	263	251	4.56
2	–	537	–
3	889	874	1.69
4	1289	1282	0.54
5	1774	1771	0.17

A dynamic response of a simply supported sandwich beam, without SMA wires, is analyzed in order to get further validation of the present finite element model. Lam and Chun [38] analyzed the dynamic response of sandwich beam subjected to impulse loading using the superposition of the normal modes. The sandwich beam consists of isotropic face sheets and orthotropic core and its material and geometrical properties are:

$L = 91.44$ cm, $c = 1.27$ cm, $h_t = h_b = 0.045$ cm, $b = 2.54$ cm

$E_c = 201.74$ MPa, $G_c = 82.68$ MPa, $\rho_c = 32.8$ kg/m^3

$E_t = E_b = 6980$ MPa, $\upsilon_t = \upsilon_b = 0.25$, $\rho_t = \rho_b = 2680$ kg/m^3

The sandwich beam is subjected to impulse load over the top surface of the beam. The load is assumed to be uniform pressure having the intensity expressed as follows:

$$P(t) = 68.9\left(1 - \frac{t}{0.004}\right)\exp\left(-\frac{1.98}{0.004}t\right)(kPa) \tag{43}$$

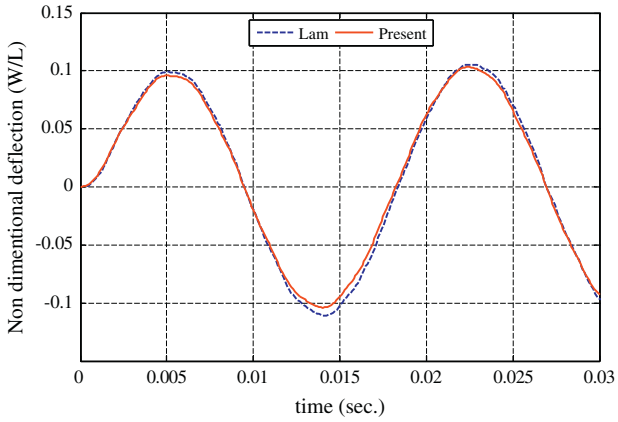

Fig. 5. Time history of deflection at the center of the top face sheet.

The deflection at the center of the top face sheet is shown in Fig. 5. As can be seen, the results of the present model are in good agreement with the results obtained analytically by Lam and Chun. It must be noticed that the theory that is used by Lam and Chun underestimates the global stiffness of the sandwich beam. For example the fundamental natural frequency obtained by this model is 57.28 Hz [38], which is less than the frequency obtained by 3D model (57.724 Hz, result of ABAQUS software done by the authors).

Example 2. In order to verify the proposed dynamic phase transformation algorithm, the dynamic response of SMA beam is investigated. In this regard, by neglecting the core of the sandwich beam and considering some manipulations, the problem is reduced to the SMA beam. Zbiciak in Ref. [3] studied the dynamic response of a pseudoelastic SMA beam based on the rheological model of SMA material with the assumption that the material properties are constant. Therefore, to enable the comparison, in the present model, the material properties are considered to be constant and the present results are compared with the results obtained by Zbiciak [3].

As shown in Fig. 6, to increase the accuracy of the results for SMA beam, the cross-section of the beam has to be divided into N layers and the calculations of the phase transformation must be accomplished for each layer individually, after which the results are superimposed. The material properties and geometrical parameters are presented in Table 2.

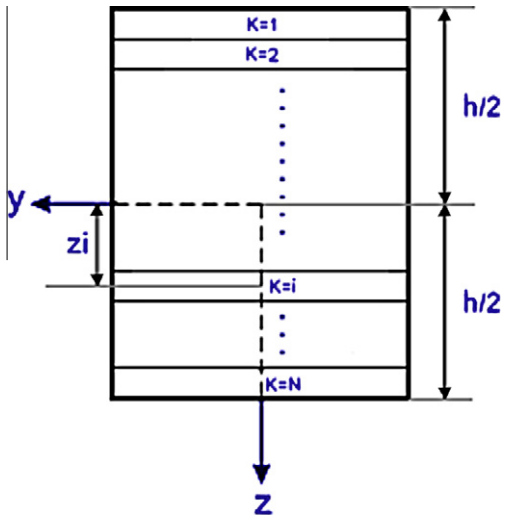

Fig. 6. Discretized layers at the cross-section of the SMA beam.

Table 2
Geometrical parameters and material properties of the SMA beam [5].

$x = 0$	Clamped
$x = L$	Simply supported
$L = 1$ m, $h = 0.08$ m, $b = 0.05$ m	
$E = 50$ GPa, $\sigma^{Ms} = 350$ MPa, $\sigma^{As} = 150$ MPa	

The SMA beam is subjected to a step impulse load at the center of the beam, having the intensity expressed as follows:

$$f(t) = 100 \text{ kN if } t \leqslant 0.05 \quad \text{and} \quad 0 \text{ kN if } t > 0.05. \tag{44}$$

A uniform 20 elements mesh is employed along the length of the beam and the cross-section of the beam is divided into 30 layers. The deflection at the center of the beam is shown in Fig. 7. As can be seen, the results of the present model are reasonably in good agreement with the results obtained by Ref. [3]. The maximum discrepancy is less than 8%. The discrepancies are mainly due to the different solution procedures. Specially, in Ref. [3], the finite difference method (FDM) along with Runge–Kutta method is used for solving the problem. Therefore, the deviations of the predicted structural stiffness with respect to the exact stiffness may be remarkable for FDM. For this reason, the response and also the period time resulted by FDM is different in comparison to the present model. It must be noted that, in Ref. [3], only the flexural equation has been solved, while in the present model, the membrane equation is also considered.

Example 3. In this example, the dynamic response of the sandwich beam with SMA composite hybrid face sheets and flexible core is investigated. In this study, the effects of the phase transformation (such as variation of material properties and dissipation of energy due to hysteresis loop) on every point along the beam are considered. The face sheets of the sandwich beam have a$[0°/90°/90°/0°]_s$ lamination sequence for each face sheet and are numbered from the top to the bottom layer for each face sheet individually. The material properties of the composite medium are presented in Table 3 and the geometrical parameters and the material properties of the core are:

$$L = 1 \text{ m}, \; c = 0.1 \text{ m}, \; h_t = h_b = 0.03 \text{ m}, \; b = 0.1 \text{ m}$$

$$E_c = 85 \text{ MPa}, \; G_c = 32.69 \text{ MPa}, \; \rho_c = 100 \text{ kg/m}^3$$

The material properties of SMA wires are presented in Table 4. In this section, the SMA wires embedded parallel to the fibers of the composite medium in the layers 1 and 8 (top and bottom layers) for both the face sheets and the volume fraction of SMA wires is 40% for each layer. As mentioned earlier, the SMA wires embedded only parallel to the fibers of the composite medium. If the

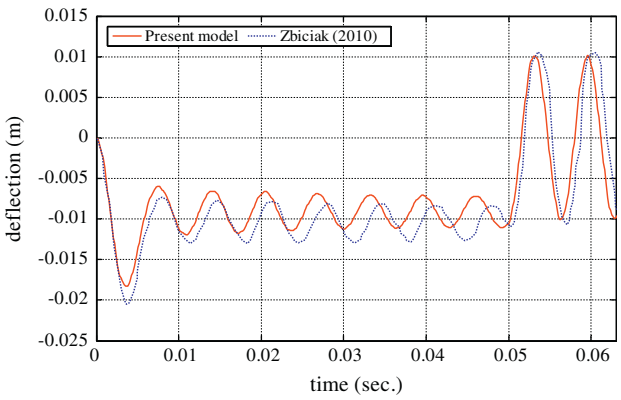

Fig. 7. Time history of deflection at the center of the SMA beam.

Table 3
Material properties of carbon/epoxy (AS4/3501-6) [40].

E_1 (N/m^2)	$E_2 = E_3$ (N/m^2)	$G_{12} = G_{13}$ (N/m^2)	G_{23} (N/m^2)	υ_{12}	ρ (kg mm^3)
144.8e9	9.65e9	4.14e9	3.45e9	0.3	1389.23

Table 4
Material properties of Nitinol alloy [30].

E_a = 67 GPa	T = 50 °C	C_M = 8 MPa/°C
E_M = 26.3 GPa	M_f = 9 °C	C_A = 13.8 MPa/°C
σ_s^{cr} = 100 MPa	M_s = 18.4 °C	
σ_f^{cr} = 170 MPa	A_s = 34.5 °C	
ε_L = 0.067	A_f = 49 °C	

orientation of the SMA wires is not the same as the direction of the composite medium fibers, the orientation mismatching of the fibers and the SMA wires causes some non fiber spaces, which contain only the brittle resin. This phenomenon causes brittle fracture and results in the reduction of structure properties [39]. The edges are simply supported and a uniform step impulse pressure with the amplitude of P = 4 MPa is applied over the upper surface of the sandwich beam.

Fig. 8 shows the stress–strain response of 1th layer of the top face sheet taking into account the pseudoelastic behavior of SMA wires. As can be seen, the stress–strain curve shows the hysteresis loops. In Fig. 9, the corresponding time history of deflection at the center of the top face sheet is shown. As can be seen in these figures, the vibration amplitude decreases gradually, such that at the time t = 0.1 s, the amplitude reaches to a value which is about 70% of its value at the first peak (t = 0.0041 s). In fact, this is due to the effect of hysteresis which dissipates the energy after each loop. Also, from Fig. 8, it is observed that as the beam oscillates, the area of dissipated energy decreases and consequently the rate of reduction in vibration amplitudes decreases. The vibration continues till the stress–strain behavior reaches the linear condition and after this point, the beam oscillates with constant amplitude and further reduction in vibration amplitude cannot be observed. In other words, due to the hysteresis of the SMA wires, the amplitude of the vibration response tends to decrease, till it is approaching to the elastic conditions of the wires and after this limit, it shows a uniform continuous response.

Fig. 10 shows the time history of martensite volume fraction (MVF) of the SMA wires for the 1st layer at the center of the top face sheet. As can be seen, during the loading process, the phase transformation initiates at t = 0.0015 s, when the stress reaches the critical martensite start stress, σ^{Ms}, (point B in Fig. 8). This

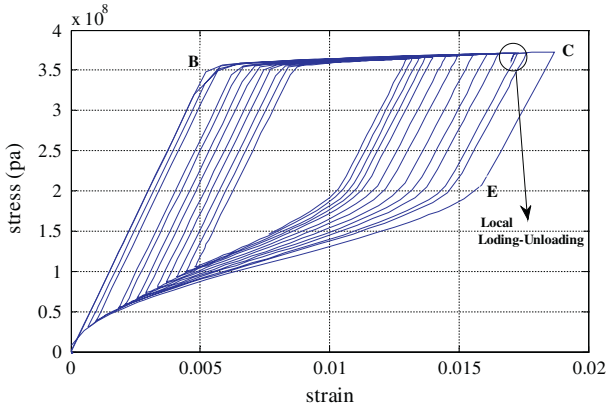

Fig. 8. The hysteresis loops at the center of the top face sheets.

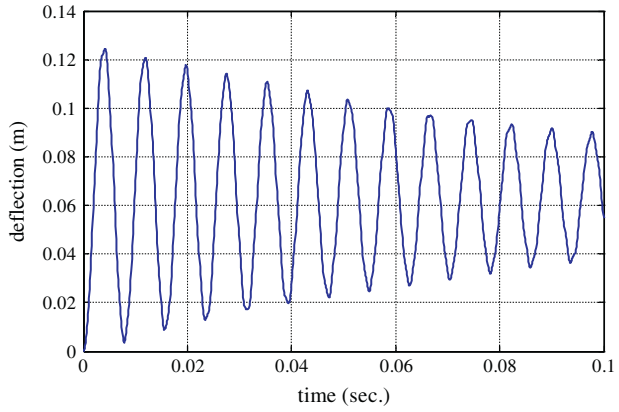

Fig. 9. Time history of deflection at the center of the top face sheet.

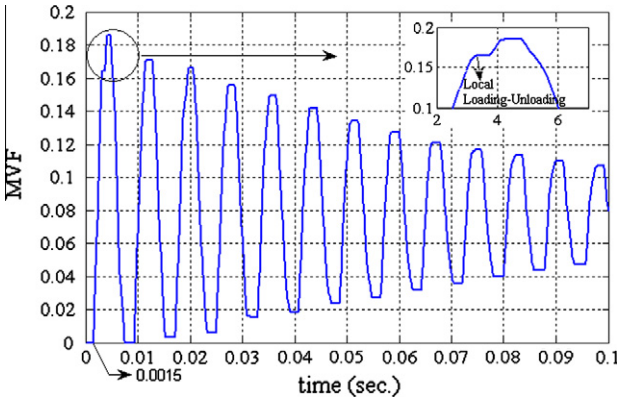

Fig. 10. Time variations of the MVF at the center of the top face sheet.

procedure continues up to the end of the loading process (t = 0.0041 s, point C in Fig. 8). As can be observed in Fig. 10, after this point is reached, a part of the curve changes to a flat state. This is due to the unloading process which begins at this point and till approaching the critical austenite start stress, σ^{As} (point E in Fig. 8), the reverse transformation does not take place. It must be noted that, before the loading or unloading processes completed, some local loading–unloading phenomenon may occur, as can be seen in Figs. 8 and 10.

This part deals with the effect of the through thickness location of the SMA wires inside the composite face sheets. In this regard, each individual face sheet consists of $[0^\circ]_8$ scheme lamination. The volume fraction of SMA wires is 40% for each layer and they are embedded in only two layers for each face sheets symmetrically. Three cases are studied. In the first case SMA wire are embedded in the layers 1 and 8 for both face sheets. In the second case SMA wires are embedded in layers 2, 7 and in the last case SMA wires are embedded in the layers 3 and 6. The counting is from top layer to bottom layer. Fig. 11 shows the effect of through thickness location of the SMA wires in the face sheets. As can be seen, when the SMA wires are embedded in the outer layers, they exhibit higher capability in damping the vibration response. In the other word, when the SMA wires embedded near the neutral axes of the face sheets, they cannot have a beneficial capability in damping the vibration response, such that when the SMA wires are embedded in the layers 3 and 6, they cannot have any damping effect. The reason of this phenomenon is that the magnitude of the stress in these layers does not reach its critical value for transformation. Therefore, in order to access the best results, the SMA wires must be embedded in the outer layers.

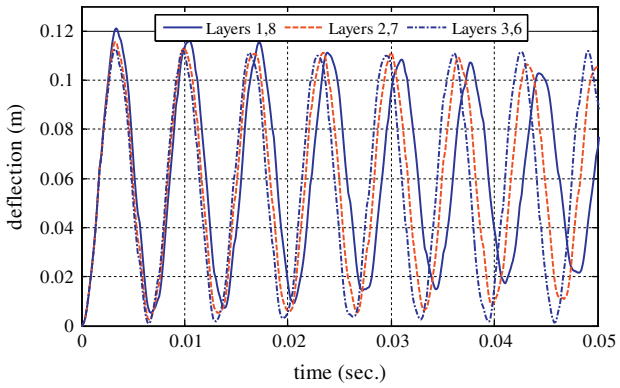

Fig. 11. Time history of deflection at the center of the top face sheet for various locations of the SMA wires.

Boundary conditions can have a significant effect on the dynamic response of the sandwich beam. The results from the present model are shown in Fig. 12. The boundary conditions SS and CC are studied in this investigation, in which S and C indicate simply supported and clamped boundary conditions, respectively. The lamination sequences of the face sheets are similar to the first part of this example. Damping ratio of the SMA hybrid composite sandwich beams could be evaluated by measuring the vibration amplitude during the vibration and using a damping equation (Eq. (45)).

$$\zeta = \frac{1}{2\pi}\frac{1}{n}\ln\left(\frac{x_1 - x_{mean}}{x_{n-1} - x_{mean}}\right) \tag{45}$$

As expected, the rigidity of the supports has a significant effect on the response of the beam. The response amplitude reaches the highest value for the SS boundary condition as compared to the lowest value for the CC boundary condition. The damping ratio of the vibration response is about 0.75% and 1.5%, for SS and CC boundary conditions, respectively. Therefore, as the rigidity of support increases, the SMA wires exhibit higher capability in damping the vibration response.

Example 4. One of the most often encountered dynamic problems in structures is the undesirable vibrations. It is known that, if a structure oscillates under conditions in which loading frequency is identical with the natural frequency of the structure, the system reaches the resonance conditions. By virtue of the hysteresis-induced damping effect and variation of Young's modulus, shape memory alloys are good viable candidate to overcome this problem. In this regard, the face sheets of the sandwich beam have a [0°/90°/90°/0°] lamination sequence for each face sheet. The SMA wires embedded parallel to the fibers of the composite medium in the layers 1 and 8 of the both face sheets and the volume fraction of SMA wires is 60% for each layer. The material and geometrical properties of the SMA composite hybrid sandwich beam are similar to example 3.

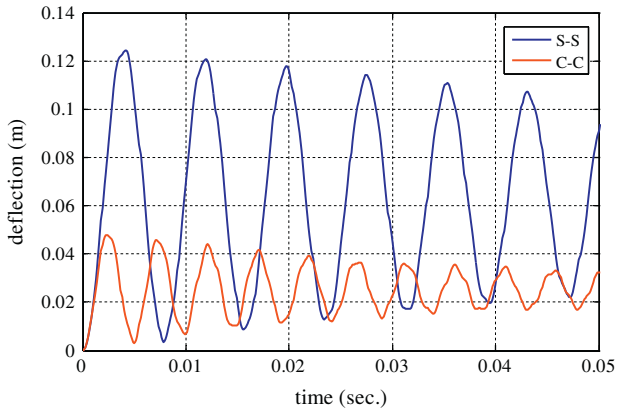

Fig. 12. Time history of deflection at the center of the top face sheet for different boundary conditions.

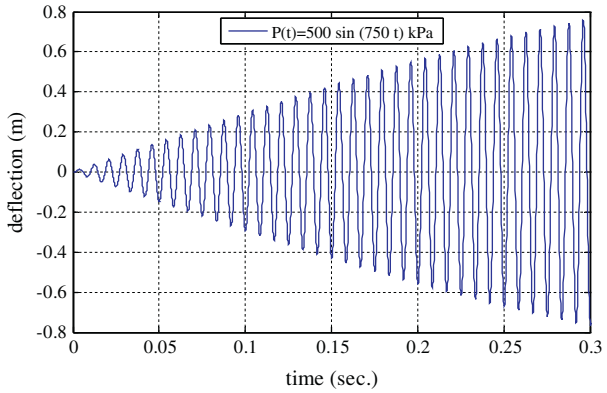

Fig. 13. Time history of deflection at the center of the top face sheet under sinusoidal loading (phase transformation effect is not considered).

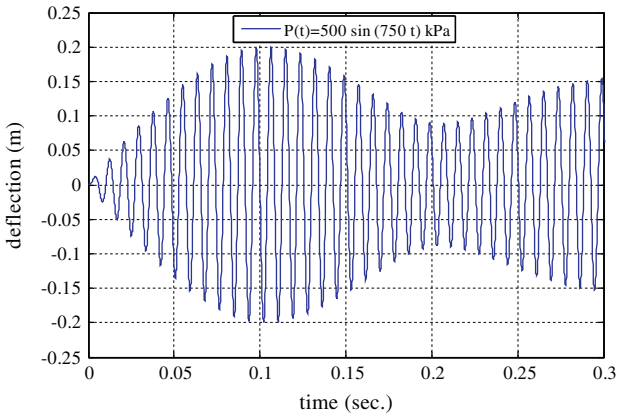

Fig. 14. Time history of deflection at the center of the top face sheet under sinusoidal loading (phase transformation effect is considered).

Having the identical elastic module at the austenite and martensite phases and also not considering the pseudoelastic effect as appeared in some performed researches, under conditions in which the loading frequency is identical to the beam's fundamental natural frequency, leads to Fig. 13, which shows a resonance conditions. While, having a different elastic modulus and considering energy dissipation, Fig. 14 demonstrates the fact that, as the amplitude increases, it shifts toward the martensite phase, and the amplitude diminishes due to the energy dissipation as well as changes in elastic modulus, and the system continues to oscillate without going into the resonance conditions.

5. Conclusion

The present research, has considered the non-linear dynamic analysis of sandwich beam with pseudoelastic SMA hybrid composite face sheets and flexible core, by taking into account the phase transformation effects, for every point along the face sheets. Due to the phase transformation the equations of motion are coupled with the kinetic equations of phase transformation of SMA wires. A new element is proposed based on the high order sandwich panel theory and a new iterative incremental finite-element-based

solution procedure is developed to solve the highly non-linear equations. The Newmark time integration method is used in solving the dynamic finite element equations. To assess the performance of the procedure developed, dynamic response of the sandwich beam with pseudoelastic SMA hybrid composite face sheets subjected to impulse load is analyzed. Results showed the efficiency of the proposed model and the relevant solution algorithm.

According to the numerical results, several most significant concluding remarks are listed as follows:

- Comparison of the free vibration analysis with experimental results shows the accuracy of the high order finite element modeling.
- It clearly appears that the dynamical behavior of the sandwich beam with pseudoelastic SMA hybrid composite face sheets is highly non-linear.
- The pseudoelastic behavior of SMA is a unique hysteresis energy-dissipation behavior, which makes the SMA wires a viable candidate for passive vibration control of sandwich structures.
- By increasing the rigidity of the supports from SS to CC, the structural capability for damping the vibration response increases.
- When the SMA wires are embedded in the outer layers of the face sheets, they exhibit higher capability in damping the vibration response.
- The material non-linearity of the SMAs is a unique behavior, which makes SMA wires a viable candidate to overcome the resonance phenomenon of sandwich structures.

Appendix A

The element mass matrix is:

$$[M^e] = \begin{bmatrix} [M_{11}^{tt}] & [M_{11}^{tb}] & [M_{12}^{tt}] & [M_{12}^{tb}] \\ [M_{11}^{bt}] & [M_{11}^{bb}] & [M_{12}^{bt}] & [M_{12}^{bb}] \\ [M_{21}^{tt}] & [M_{21}^{tb}] & [M_{22}^{tt}] & [M_{22}^{tb}] \\ [M_{21}^{bt}] & [M_{21}^{bb}] & [M_{22}^{bt}] & [M_{22}^{bb}] \end{bmatrix}$$

$$[M_{11}^{tt}] = -\int_{x1}^{x2} \left[\left(I_{0t} + \frac{m_c}{3}\right)\psi^T\psi\right] dx$$

$$[M_{11}^{tb}] = -\int_{x1}^{x2} \left[\left(\frac{m_c}{6}\right)\psi^T\psi\right] dx$$

$$[M_{12}^{tt}] = \int_{x1}^{x2} \left[\left(\frac{m_c h_t}{6}\right) + I_{1t}\right]\psi^T \frac{\partial\phi}{\partial x}\, dx$$

$$[M_{12}^{tb}] = -\int_{x1}^{x2} \left[\left(\frac{m_c h_b}{6}\right)\right]\psi^T \frac{\partial\phi}{\partial x}\, dx$$

$$[M_{11}^{bb}] = -\int_{x1}^{x2} \left[\left(I_{0b} + \frac{m_c}{3}\right)\psi^T\psi\right] dx$$

$$[M_{11}^{bt}] = -\int_{x1}^{x2} \left[\left(\frac{m_c}{6}\right)\psi^T\psi\right] dx$$

$$[M_{12}^{bb}] = -\int_{x1}^{x2} \left[\left(\frac{m_c h_b}{6}\right) - I_{1b}\right]\psi^T \frac{\partial\phi}{\partial x}\, dx$$

$$[M_{12}^{bt}] = -\int_{x1}^{x2} \left[\left(\frac{m_c h_t}{12}\right)\right]\psi^T \frac{\partial\phi}{\partial x}\, dx$$

$$[M_{22}^{tt}] = -\int_{x1}^{x2} \left[\left(\frac{m_c h_t^2}{12} + I_{2t}\right)\frac{\partial\phi^T}{\partial x}\frac{\partial\phi}{\partial x} + \left(\frac{m_c}{3} + I_{0t}\right)\right]\phi^T\phi\, dx$$

$$[M_{22}^{tb}] = \int_{x1}^{x2} \left[\left(\frac{m_c h_t h_b}{24}\right)\frac{\partial\phi^T}{\partial x}\frac{\partial\phi}{\partial x} - \left(\frac{m_c}{6}\right)\phi^T\phi\right] dx$$

$$[M_{21}^{tt}] = \int_{x1}^{x2} \left[\left(\frac{m_c h_t}{6} + I_{1t}\right)\right]\frac{\partial\phi^T}{\partial x}\psi\, dx$$

$$[M_{21}^{tb}] = \int_{x1}^{x2} \left[\left(\frac{m_c h_t}{12}\right)\frac{\partial\phi^T}{\partial x}\psi\right] dx$$

$$[M_{22}^{bb}] = -\int_{x1}^{x2} \left[\left(\frac{m_c h_b^2}{12} + I_{2b}\right)\frac{\partial\phi^T}{\partial x}\frac{\partial\phi}{\partial x} + \left(\frac{m_c}{3} + I_{0b}\right)\right]\phi^T\phi\, dx$$

$$[M_{22}^{bt}] = \int_{x1}^{x2} \left[\left(\frac{m_c h_t h_b}{24}\right)\frac{\partial\phi^T}{\partial x}\frac{\partial\phi}{\partial x} - \left(\frac{m_c}{6}\right)\phi^T\phi\right] dx$$

$$[M_{21}^{bb}] = \int_{x1}^{x2} \left[\left(-\frac{m_c h_b}{6} + I_{1b}\right)\right]\frac{\partial\phi^T}{\partial x}\psi\, dx$$

$$[M_{21}^{bt}] = \int_{x1}^{x2} \left[\left(-\frac{m_c h_b}{12}\right)\frac{\partial\phi^T}{\partial x}\psi\right] dx$$

The element stiffness matrix is:

$$[K^e] = \begin{bmatrix} [K_{11}^{tt}] & [K_{11}^{tb}] & [K_{12}^{tt}] & [K_{12}^{tb}] & [K_{13}^{t}] \\ [K_{11}^{bt}] & [K_{11}^{bb}] & [K_{12}^{bt}] & [K_{12}^{bb}] & [K_{13}^{b}] \\ [K_{21}^{tt}] & [K_{21}^{tb}] & [K_{22}^{tt}] & [K_{22}^{tb}] & [K_{23}^{t}] \\ [K_{21}^{bt}] & [K_{21}^{bb}] & [K_{22}^{bt}] & [K_{22}^{bb}] & [K_{23}^{b}] \\ [K_{31}^{t}] & [K_{31}^{b}] & [K_{32}^{t}] & [K_{32}^{b}] & [K_{33}] \end{bmatrix}$$

$$[K_{11}^{tt}] = -\int_{x1}^{x2} \left[A^t(\xi)\frac{\partial\psi^T}{\partial x}\frac{\partial\psi}{\partial x}\right] dx$$

$$[K_{12}^{tt}] = \int_{x1}^{x2} \left[B^t(\xi)\frac{\partial\psi^T}{\partial x}\frac{\partial^2\phi}{\partial x^2}\right] dx$$

$$[K_{13}^{t}] = \int_{x1}^{x2} [b\psi^T\psi]\, dx$$

$$[K_{11}^{bb}] = -\int_{x1}^{x2} \left[A^b(\xi)\frac{\partial\psi^T}{\partial x}\frac{\partial\psi}{\partial x}\right] dx$$

$$[K_{12}^{bb}] = \int_{x1}^{x2} \left[B^t(\xi)\frac{\partial\psi^T}{\partial x}\frac{\partial^2\phi}{\partial x^2}\right] dx$$

$$[K_{13}^{b}] = -\int_{x1}^{x2} [b\psi^T\psi]\, dx$$

$$[K_{22}^{tt}] = \int_{x1}^{x2} \left[-D^t(\xi)\frac{\partial^2\phi^T}{\partial x^2}\frac{\partial^2\phi}{\partial x^2} - \frac{bE_c}{c}\phi^T\phi\right] dx$$

$$\left[K_{22}^{tb}\right] = \int_{x1}^{x2} \left[\frac{bE_c}{c}\phi^T\phi\right]dx$$

$$\left[K_{21}^{tt}\right] = \int_{x1}^{x2} \left[B^t(\xi)\frac{\partial^2\phi^T}{\partial x^2}\frac{\partial\psi}{\partial x}\right]dx$$

$$\left[K_{23}^{t}\right] = \int_{x1}^{x2} \left[\frac{-b(h_t+c)}{2}\frac{\partial\phi^T}{\partial x}\psi\right]dx$$

$$\left[K_{22}^{bb}\right] = \int_{x1}^{x2} \left[-D^b(\xi)\frac{\partial^2\phi^T}{\partial x^2}\frac{\partial^2\phi}{\partial x^2} - \frac{bE_c}{c}\phi^T\phi\right]dx$$

$$\left[K_{22}^{bt}\right] = \int_{x1}^{x2} \left[\frac{bE_c}{c}\phi^T\phi\right]dx$$

$$\left[K_{21}^{bb}\right] = \int_{x1}^{x2} \left[B^b(\xi)\frac{\partial^2\phi^T}{\partial x^2}\frac{\partial\psi}{\partial x}\right]dx$$

$$\left[K_{23}^{b}\right] = \int_{x1}^{x2} \left[\frac{-b(h_t+c)}{2}\frac{\partial\phi^T}{\partial x}\psi\right]dx$$

$$\left[K_{31}^{t}\right] = \int_{x1}^{x2} \left[b\psi^T\psi\right]dx$$

$$\left[K_{31}^{b}\right] = -\int_{x1}^{x2} \left[b\psi^T\psi\right]dx$$

$$\left[K_{32}^{t}\right] = \int_{x1}^{x2} \left[\frac{-b(h_t+c)}{2}\psi^T\frac{\partial\phi}{\partial x}\right]dx$$

$$\left[K_{32}^{b}\right] = \int_{x1}^{x2} \left[\frac{-b(h_b+c)}{2}\psi^T\frac{\partial\phi}{\partial x}\right]dx$$

$$\left[K_{33}\right] = \int_{x1}^{x2} \left[\frac{bc^3}{E_c}\frac{\partial\psi^T}{\partial x}\frac{\partial\psi}{\partial x} + \frac{bc}{G_c}\psi^T\psi\right]dx$$

The rest of sub-matrices that are not defined are null matrix.

The element force vector is:

$$\{F^e\} = \left\{\{F_1^t\}\left\{F_1^b\right\}\{F_2^t\}\left\{F_1^b\right\}\{F_3\}\right\}$$

$$\{F_1^t\} = -\psi^T(x_2)N_{xx}^t(x_2) + \psi^T(x_1)N_{xx}^t(x_1) + \int_{x1}^{x2}\frac{\partial\psi^T}{\partial x}\mathrm{A}_{xxs}^t(\xi)dx$$

$$\left\{F_1^b\right\} = -\psi^T(x_2)N_{xx}^b(x_2) + \psi^T(x_1)N_{xx}^b(x_1) + \int_{x1}^{x2}\frac{\partial\psi^T}{\partial x}\mathrm{A}_{xxs}^b(\xi)dx$$

$$\{F_2^t\} = \phi^T(x_1)Q^t(x_1) - \phi^T(x_2)Q^t(x_2) + \tfrac{\partial\phi^T(x_1)}{\partial x}M_{xx}^t(x_1) - \tfrac{\partial\phi^T(x_2)}{\partial x}M_{xx}^t(x_2) - \int_{x1}^{x2}\left[\tfrac{\partial^2\phi^T}{\partial x^2}B_{xxs}^t(\xi)\right]dx - \int_{x1}^{x2}[b\phi^T q_t]dx$$

$$\left\{F_2^b\right\} = \phi^T(x_1)Q^t(x_1) - \phi^T(x_2)Q^t(x_2) + \tfrac{\partial\phi^T(x_1)}{\partial x}M_{xx}^b(x_1) - \tfrac{\partial\phi^T(x_2)}{\partial x}M_{xx}^b(x_2) - \int_{x1}^{x2}\left[\tfrac{\partial^2\phi^T}{\partial x^2}B_{xxs}^b(\xi)\right]dx - \int_{x1}^{x2}[b\phi^T q_b]dx$$

$$\{F_3\} = \frac{bc^3}{E_c}\left[\psi^T(x_2)\frac{\partial\tau(x_2)}{\partial x} - \psi^T(x_1)\frac{\partial\tau(x_1)}{\partial x}\right]$$

The vector of the nodal values is:

$$\{\Delta^e\} = \{\{U^t\}\{W^t\}\{U^b\}\{W^b\}\{\tau\}\}$$

References

[1] Hashemi SMT, Khadem SE. Modeling and analysis of the vibration behavior of a shape memory alloy beam. Int J Mech Sci 2006;48:44–52.

[2] Jafari AA, Ghiasvand H. Dynamic response of a pseudoelastic shape memory alloy beam to a moving load. J Sound Vib 2008;316:69–86.

[3] Zbiciak A. Dynamic analysis of pseudoelastic SMA beam. Int J Mech Sci 2010;52:56–64.

[4] Rogers CA, Barker DK. Experimental studies of active strain energy tuning of adaptive composites. In: Proc. AIAA/ASME/ASCE/AHS/ASC 31st structures, structural dynamics, and materials conf., Long Beach, CA, April 1990.

[5] Baz A, Imam K, McCoy J. Active vibration control of flexible beams using shape memory actuators. J Sound Vib 1990;140(3):437–56.

[6] Baz A, Ro J, Mutua M, Gilheany J. Active buckling control of Nitinol-reinforced composite beams. In: Conf. active material and adaptive structures (Alexandria, VA), November 1991. p. 167–76.

[7] Chen Q, Levy C. Active vibration control of elastic beams by means of shape memory alloy layers. Smart Mater Struct 1996;5:400–6.

[8] Epps J, Chandra R. Shape memory alloy actuation for active tuning of composite beams. Smart Mater Struct 1997;6:251–64.

[9] Ghomshei MM, Tabandeh N, Ghazavi A, Gordaninejad F. Nonlinear transient response of a thick composite beam with shape memory alloy layers. Compos Part B: Eng 2005;36:9–24.

[10] Khalili SMR, Shokuhfar A, Malekzadeh K, Ghasemi FA. Low-velocity impact response of active thin-walled hybrid composite structures embedded with SMA wires. Thin-Walled Struct 2007;45:799–808.

[11] Khalili SMR, Shokuhfar A, Ghasemi FA. Effect of smart stiffening procedure on low-velocity impact response of smart structures. J Mater Process Technol 2007;190:142–52.

[12] Lu P, Cui FS, Tan MJ. A theoretical model for the bending of a laminated beam with SMA fiber embedded layer. Compos Struct 2009;90:458–64.

[13] Carrera E, Brischetto S. A survey with numerical assessment of classical and refined theories for the analysis of sandwich plates. Appl Mech Rev 2009;62(010803):1–17.

[14] Noor AK, Burton S, Bert CW. Computational model for sandwich panels and shells. Appl Mech Rev 1996;49:155–99.

[15] Ditaranto RA. Theory of vibratory bending for elastic and viscoelastic layered finite length beams. J Appl Mech 1965;32(4):881–6.

[16] Mead DJ, Markus S. The forced vibration of a three-layer damped sandwich beam with arbitrary boundary condition. J Sound Vib 1969;10(2):63–75.

[17] Mead DJ. A comparison of some equations for the flexural vibration of damped sandwich beams. J Sound Vib 1982;83(3):63–77.

[18] Ahmed KM. Free vibration of curved sandwich beams by the method of finite elements. J Sound Vib 1971;18(1):61–74.

[19] Banerjee JR, Cheung CW, Morishima R, Perera M, Njuguna J. Free vibration of a three layered sandwich beam using the dynamic stiffness method and experiment. Int J Solids Struct 2007;44:7543–63.

[20] Khalili SMR, Nemati N, Malekzadeh K, Damanpack AR. Free vibration analysis of sandwich beams using improved dynamic stiffness method. Compos Struct 2010;92:387–94.

[21] Frostig Y, Baruch M. Free vibration of sandwich beams with a transversely flexible core: a hight order approach. J Sound Vib 1994;176(2):195–208.

[22] Sokolinsky VS, Nutt SR, Frostig Y. Boundary condition effects in free vibrations of higher-order soft sandwich beams. AIAA J 2002;40(6):1220–7.

[23] Sokolinsky VS, Nutt SR. Consistent higher-order dynamic equations for soft-core sandwich beams. AIAA J 2004;42(2):374–82.

[24] Sokolinsky VS, Von Bremen HF, Lavoie JA, Nutt SR. Analytical and experimental study of free vibration response of soft-core sandwich beams. J Sandwich Struct Mater 2004;6:230–61.

[25] Khalili MR, Malekzadeh K, Mittal RK. Effect of physical and geometrical parameters on transverse low velocity impact response of sandwich panels with a transversely flexible core. Compos Struct 2007;77:430–43.

[26] Malekzadeh K, Khalili MR, Mittal RK. Local and global damped vibrations of sandwich plates with a viscoelastic soft flexible core: an improved high-order approach. J Sandwich Struct Mater 2005;7(5):431–56.

[27] Yang M, Qiao P. Higher-order impact modeling of sandwich structures with flexible core. Int J Solids Struct 2005;42:5460–90.

[28] Birman V. Stability of functionally graded shape memory alloy sandwich panels. Smart Mater Struct 1997;6:278–86.

[29] Brinson LC, Lammering R. Finite element analysis of the behavior of shape memory alloys and their applications. Int J Solids Struct 1993;30(23):3261–80.

[30] Brinson LC. One-dimensional constitutive model of shape memory alloys: thermomechanical derivation with non-constant material functions. J Intell Mater Syst Struct 1993;4(2):229–42.

[31] Lagoudas DC. Shape memory alloys, modeling and engineering applications. USA: Springer; 2008.

[32] Reddy JN. Principle of energy and variational methods in applied mechanic. Hoboken (New Jersey): John Wily & Sons; 2000.

[33] Birman V, Chandrashekhara K, Sain S. An approach to optimization of shape memory alloy hybrid composite plates subjected to low velocity impact. Compos Part B: Eng 1996;27B:439–46.

[34] Frostig Y. Behavior of delaminated sandwich beam with transversely flexible core-high order theory. Compos Struct 1992;20(1):1–16.

[35] Huebner KH, Dewhirst DL, Smith DE, Byrom TG. The finite element method for engineers. 4th ed. Wiley; 2001.

[36] Reddy JN. An introduction to nonlinear finite element analysis. New York: Oxford University Press; 2004.
[37] Jensen AE, Irgens F. Thickness vibrations of sandwich plates and beams and delamination detection. J Intell Mater Syst Struct 1999;10(1):46–55.
[38] Lam KY, Chun L. Dynamics response of a simply supported sandwich beam subjected to impulsive loading. Compos Struct 1994;27:331–7.
[39] Tsoi KA, Stalmans R, Schrooten J, Mai YW. Impact damage behavior of shape memory alloy composites. Mater Sci Eng Part A 2003;342:207–15.
[40] Chandrashekhara K, Krisnamurty K, Roy S. Free vibration of composite beams including rotary inertia and shear deformation. Compos Struct 1990;14: 269–79.